

# Dependence of R2\* bias on through-voxel frequency dispersion and gradient echo train in high-resolution 3D R2\* mapping

G. Helms<sup>1</sup>, and P. Dechent<sup>1</sup>

<sup>1</sup>MR-Research in Neurology and Psychiatry, University Medical Center, Göttingen, Lower Saxony, Germany

## Introduction:

The effective rate of decay of transverse magnetization,  $R2^* = 1/T2^*$ , is sensitive to  $B_0$  distortions at a mesoscopic scale (1). It is thus highly correlated to tissue concentrations of non-heme iron (2) and myelinated axons (3), especially at high and ultra-high field strengths (2-4).  $R2^*$  is commonly measured using long-TR multi-slice gradient echo sequences. This approach implies high SNR and long echo trains, but limited resolution and increased sensitivity to through-voxel gradients in the slice direction. The latter have been modelled by linear dispersion imposing a sinc modulation on the exponential  $T2^*$  decay (5). However, many fiber tracts and iron-containing nuclei involved in motor disease (like substantia nigra and subthalamic nucleus (6)) have a double-oblique orientation, so  $R2^*$  measurements may be compromised by a 2D approach. 3D measurements at isotropic high resolution is also desirable for voxel-based statistical approaches (7) requiring spatial normalization. Here, the time required for the additional phase-encoding constrains TR and thus the duration of the gradient-echo train. Therefore, the behaviour of sinc model was studied for constraints of short gradient-echo train to guide the implementation of 3D  $R2^*$  mapping scheme.

## Theory and simulations:

The modulation of the sinc function is parameterized by the frequency dispersion  $\Delta\nu = \gamma G \Delta x$  (in Hz/pixel) of a through-plane gradient  $G$  along the voxel dimension  $\Delta x$ . Up to the first root (or "node"), it is excellently approximated by its Taylor expansion:

$$\text{sinc}(\Delta\nu\text{TE}) = \sin(\pi\Delta\nu\text{TE})/(\pi\Delta\nu\text{TE}) \approx 1 - (\pi\Delta\nu\text{TE})^2/6 + (\pi\Delta\nu\text{TE})^4/6/20 - (\pi\Delta\nu\text{TE})^6/6/20/42. \quad [1]$$

The log signals  $S(\text{TE}) = S0 \exp(R2^*\text{TE}) \text{sinc}(\Delta\nu\text{TE})$  are used,  $R2^*$  and  $\Delta\nu$  appear at different order:

$$\log(S(\text{TE})) \approx \log(S0) - R2^*\text{TE} - (\pi\Delta\nu\text{TE})^2/6 - (\pi\Delta\nu\text{TE})^4/180 - (\pi\Delta\nu\text{TE})^6/2835; \quad [2]$$

so the dephasing correction can be implemented as polynomial regression. For standard linear regression, Eq. [2] predicts an additive bias  $\Delta R2^* = R2^*(\text{fitted}) - R2^*$  that is independent of  $R2^*$  and increases with  $\Delta\nu$  if  $\Delta\nu^2$ , if  $\text{TE}_{\text{max}} \ll 1$ . Log regression with different  $R2^*$  and dispersion was simulation for TE sampling schemes reported for 3T (2-4,6,7) A steep increase of the  $\Delta R2^*$  offset was observed for if  $\Delta\nu\text{TE}_{\text{max}} \rightarrow 1$ , so  $\Delta R2^*$  was fitted empirically by:

$$\Delta R2^* = A \Delta\nu^2 / [1 - \Delta\nu\text{TE}_{\text{max}}]^B \quad [3a]$$

This was also used for the normalized S0 offset

$$\Delta S0/S0 = C \Delta\nu^2 / [1 - \Delta\nu\text{TE}_{\text{max}}]^D \quad [3b]$$

## Experimental:

3D multi-echo FLASH imaging was performed on consenting healthy adults on a 3T whole-body system (Siemens Tim Trio) using an 8-channel receive-only head coil and the body coil for transmission. First, similar to (6), 8 bipolar echoes at multiples of  $\text{TE} = 4.92$  ms with isotropic 1 mm resolution (non-selective excitation of 176 sagittal partitions, 256x176 mm field-of-view,  $\text{TR}/\alpha = 23$  ms/6°). Measuring time using 6/8 partial Fourier (phase/partition) and 2x GRAPPA (24 reference lines, phase) was 6.5 minutes, respectively.

FSL 4.0 ([www.fmrib.ox.ac.uk/fsl](http://www.fmrib.ox.ac.uk/fsl)) was used for image-processing. After brain extraction, regression of order 1, 2, and 4 was performed on the log signals. The frequency offset was calculated from unwrapped phase images. Local gradients were derived by a differentiation kernel and used to correct  $R2^*$  with parameters A and B determined by simulation.

## Results:

**Simulation:** The dispersion related offset of  $R2^*$  and S0 were independent of  $R2^*$  and excellently described by Eqs.[3a,b] (Fig.1). Thus, longer echo trains are more sensitive to frequency dispersion. The initial increase A was correlated to the shortest  $\text{TE}_{\text{min}}$ , whereas a fewer number of echoes increased the exponent B. **Experimental:** Polynomial regression introduced errors into the  $R2^*$  maps (Fig. 2) probably due to a correlation between the terms. Correction of  $R2^*$  by Eq.[3a] introduced noise or failed probably due to oblique gradients (not shown). Figure 3 shows  $R2^*$  overlays and histogram of the 3D acquisition. The high-resolution/short TE scheme yielded reliable  $R2^*$  mapping down to the level of the pons and the cerebellum SN, with excessive bias ( $R2^* > 50 \text{ sec}^{-1}$ ) only in orbito-frontal and temporo-basal regions.

## Discussion:

An empirical model for the influence of through-voxel gradients on  $R2^*$  was derived from simulations, showing how the TE sampling scheme influences the sensitivity to frequency dispersion. 3D mapping of  $R2^*$  advocates short gradient echo trains and high-resolution; thus confining the  $R2^*$  bias to rather small sub-regions. This proved to be more feasible than correction. Non-selective excitation reduces the influence of small dispersion via a short  $\text{TE}_{\text{min}}$ . Despite the general trade-off between statistical error and sensitivity to bias, high-resolution  $R2^*$  mapping of the brain seems feasible using 3D sequences at 3T.

## References:

[1] Yablonskij, Haacke. *MRM* 32:749 (1994) [2] Yao et al.; *NeuroImage* 44:1259 (2009) [3] Li et al. *MRM* ePub (2009) [4] Peters et al. *MRI* 25:748 (2007) [5] Fernández-Seara, Wehrli. *MRM* 44:358 (2000) [6] Helms et al. *Proc ISMRM* 16 (2008) [7] Péran et al. *JMRI* 26:1413 (2007)

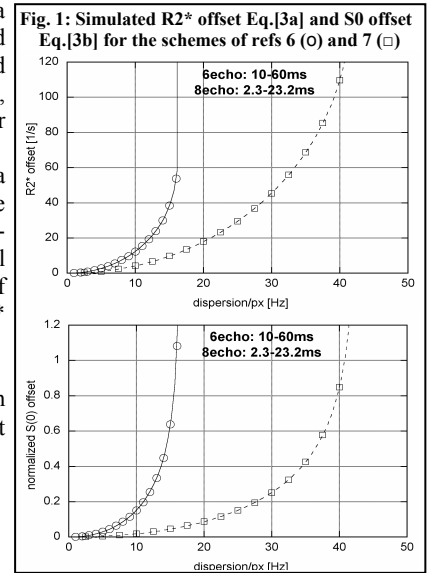


Fig. 1: Simulated  $R2^*$  offset Eq.[3a] and S0 offset Eq.[3b] for the schemes of refs 6 (O) and 7 (□)

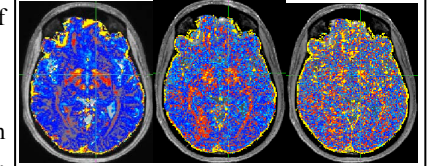


Fig. 2:  $R2^*$  noise due to polynomial regression of order 1, 2, and 4 Eq. [2]

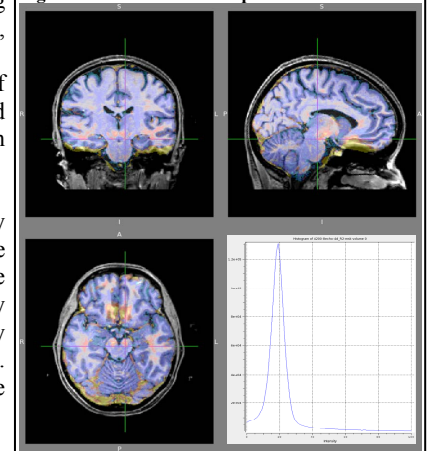


Fig. 3: Uncorrected  $R2^*$  maps at 1 mm resolution